benefits to high-pressure mineral physics and the Earth sciences in general. This will generate great collateral benefits to high-pressure mineral physics in general.

Acknowledgments

The authors acknowledge C. S. Yoo, V. V. Struzhkin, A. F. Goncharov, W. Sturhahn, J. M. Jackson, D. Yuen, and K. Hirose for stimulating discussions. This work at Lawrence Livermore National Laboratory (LLNL) was performed under the auspices of the U.S. Department of Energy by the University of California/LLNL under contract W-7405-Eng-48. S.D.J. acknowledges support from the U.S. National Science Foundation (NSF; EAR-0440112). R.M.W. also acknowledges support from NSF (EAR-0325218 and ITR-0428774).

References

Badro, J., et al. (2003), Iron partitioning in Earth's mantle: Toward a deep lower mantle discontinuity, *Science, 300*, 789–791.

Badro, J., et al. (2004), Electronic transitions in perovskite: Possible nonconvecting layers in the lower mantle, *Science, 305,* 383–386.

Goncharov, A. F., V. V. Struzhkin, and S. D. Jacobsen (2006), Reduced radiative conductivity of low-spin (Mg, Fe) O in the lower mantle, *Science, 312*, 1205–1208.

Hofmeister, A. M. (1999), Mantle values of thermal conductivity and the geotherm from phonon lifetime, *Science, 283*, 1699–1706.

Lin, J. F., et al. (2005), Spin transition of iron in magnesiowüstite in Earth's lower mantle, *Nature, 436*, 377–380.

Lin, J. F., et al. (2006), Sound velocities of ferropericlase in Earth's lower mantle, *Geophys. Res. Lett., 33,* L22304, doi:10.1029/2006GL028099.

Matyska, C., and D. A. Yuen (2006), Lower mantle dynamics with the post-perovskite phase change, radiative thermal conductivity, temperature- and depth-dependent viscosity, *Earth Planet. Sc. Lett., 154*, 196-207.

Sturhahn, W., J. M. Jackson, and J. F. Lin (2005), The spin state of iron in Earth's lower mantle minerals, *Geophys. Res. Lett., 32*, L12307.

Tsuchiya, T., R. M. Wentzcovitch, C. R. S. da Silva, and S. de Gironcoli (2006), Spin transition in magnesiowüstite in Earth's lower mantle, *Phys. Rev. Lett., 96,* 198501.

Author Information

Jung-Fu Lin, Lawrence Livermore National Laboratory, Livermore, Calif.; E-mail:lin24@llnl.gov; Steven D. Jacobsen, Department of Earth and Planetary Sciences, Northwestern University, Evanston, Ill.; and Renata M. Wentzcovitch, Department of Chemical Engineering and Materials Science, University of Minnesota, Minneapolis.

Looking Below the Moon's Surface With Radar

PAGES 13, 18

Imaging radar observations of the Moon at long wavelengths probe up to tens of meters into the mixed dust and rock of the lunar regolith. These images support geologic studies, mapping of resource-bearing deposits of pyroclastic glasses or titanium-rich basalt, and the search for safe landing sites with ready access to such resources.

A nearly complete map of the lunar nearside at 70-centimeter wavelength has been collected, using the radar transmitter on the U.S. National Science Foundation's (NSF) Arecibo telescope in Puerto Rico and receivers on the NSF's Robert C. Byrd Greenbank Telescope (GBT) in West Virginia (Figure 1). These data have been submitted to the Planetary Data System in a format that makes them useful for a variety of lunar science applications.

The Moon's surface is exposed to bombardment by large and small meteorites, and over time these impacts create a mixed layer of dust and rock fragments called the regolith. Atop the basalt flows (maria) that fill ancient basin floors, the regolith is a few meters thick. In older highlands terrain, the regolith is 10 meters or more in thickness, with significant layering that reflects overlapping ejecta deposits from the major basins and nearby large craters. Remote sensing data in ultraviolet to thermal infrared wavelengths characterize regolith physical properties and composition for the upper few microns to centimeters. Gamma ray and neutron measurements extend the depth of probing to about one meter with, to date, coarse spatial resolution.

By B. A. Campbell, D. B. Campbell, J.-L. Margot, R. R. Ghent, M. Nolan, L. M. Carter, and N. J. S. Stacy

Only the drill cores and shallow seismic and electrical surveys made by the Apollo astronauts address the vertical and horizontal variations in the regolith, and for just a few sites on the Moon. Earth-based long-wavelength imaging radar provides a window on near-surface regolith properties across the entire nearside and illustrates the scientific potential of future radar studies of Mars.

Lunar Radar Mapping

Earth-based radar maps are produced by measuring echo power as a function of time delay and Doppler shift that can be related to the different distances and velocities, relative to the radar's location, of each point on the lunar surface. The delay-Doppler ambiguity between points north and south of the 'spin equator' is avoided by pointing the Arecibo beam toward just one hemisphere of the Moon. The transmitted radar signals are adjusted to hold a single target point on the Moon at fixed time delay and frequency throughout a 16-minute 'look.' Other sites on the Moon also illuminated by the Arecibo radar signal have different delay and frequency changes with time, and so their reflected energy is 'smeared' over many resolution elements. A 'patch-focusing' technique is used to compensate for these drifts over a region centered on some particular point, and the high-resolution map is assembled from a grid of locally focused images.

The maps have a horizontal spatial resolution along the delay axis of 450 meters per pixel at the limb, and about 900 meters per pixel closer to the center of the disk. Resolution along the frequency axis is 320 meters along the apparent spin axis of the Moon and degrades slowly with increasing angular offsets from the spin vector. The data are resampled to a lunar cartographic grid at 400-meter spacing.

Arecibo transmits a circularly polarized radar signal, and the GBT is used to receive both reflected senses of circular polarization. These two channels are important because they contain information on mirror-like echoes from locally flat parts of the Moon as well as from diffuse echoes associated with rocks, roughly 10 centimeters and larger, on and within the regolith. The transmitted power and the strength of the GBT thermal noise signal are measured to allow calibration of the echoes to backscatter cross section. The circular polarization ratio (CPR) obtained from the two echo channels is a measure of decimeter-scale rock abundance and can be used to search for thick ice deposits in permanently shadowed regions near the poles. A calibrated data set allows comparison between echoes from lunar geologic features and terrain

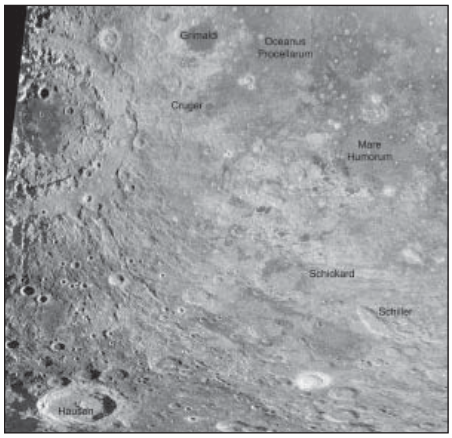

Fig. 1. Seventy-centimeter radar map of the Moon's southwest nearside (0°–70°S, 100°–27°W); same-sense circular polarization. The area of low radar return surrounding Cruger crater and extending northeast to Oceanus Procellarum is likely a deposit of ancient mare basalt buried by Orientale basin debris. The SMART-1 impact site is just south of Mare Humorum.

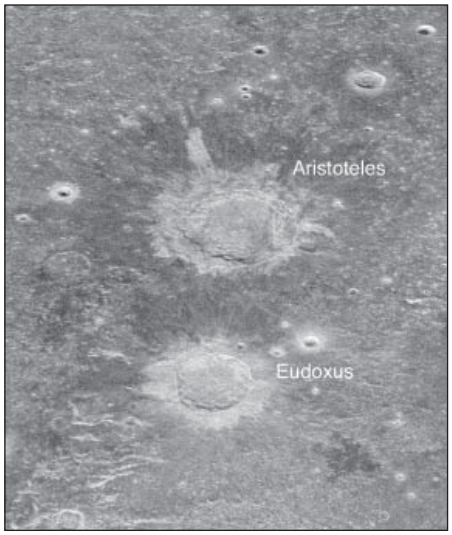

Fig. 2. Seventy-centimeter radar map of lunar craters with low-return concentric haloes; same-sense circular polarization. Aristoteles is 87 kilometers in diameter. These radar-dark haloes are attributed to rock-poor debris layers beyond the rugged proximal crater rim deposits. Over time, smaller impacts overturn the regolith, and the radar backscatter increases to that of the background highlands or maria.

observed on Earth by the NASA Jet Propulsion Laboratory airborne synthetic aperture radar (AIRSAR) system.

Geology and Resources

The new 70-centimeter radar maps provide unique insight into the physical properties of the Moon's near-surface environment. In particular, the long-wavelength signals can probe to considerable depth, depending upon the regolith rock abundance and loss properties [*Thompson,* 1987]. On Earth, radar penetration is limited to very dry locations, because even small amounts of water mixed with natural salts lead to high attenuation of the signal. Lunar rocks, formed without water, can have much lower losses and hence allow greater radar penetration. In the feldspar-rich highlands, the 70-centimeter signal can probe to depths up to 50 meters. In the regolith of the basaltic maria, the penetration depth is just a few meters and is controlled largely by the abundance of ilmenite ($FeTiO_3$) [*Carrier et al.,* 1991, *Schaber et al.,* 1975]. This is actually of great benefit, since ilmenite represents a potential lunar resource, and the link between remote sensing data and titanium-rich soils has long been a topic of research.

Comparing the 70-centimeter radar echoes to estimates of surface composition based on multispectral data from the Clementine orbiter reveals the outline of an extensive basalt deposit, connected with the larger Oceanus Procellarum, that underlies the outer ejecta of the Orientale basin [*Campbell and Hawke,* 2005]. 'Cryptomare' units have been previously identified by multispectral studies [*Mustard and Head,* 1996], but the radar offers the first chance to map their actual extent and relationship to topography (Figure 1). Such comparisons also suggest that the radar and multispectral data can distinguish the effects of titanium content and age—younger mare units have a thinner, more blocky regolith and thus a higher echo for any given ilmenite content.

The abundance of rocks on the surface and suspended in the fine dust is also important, as it reflects aspects of the impact cratering process from the local scale up to giant basin-forming events. Younger craters 10 kilometers or more in diameter have associated radar-dark 'haloes' concentric to the rough, radar-bright, near-rim ejecta (Figure 2) [*Ghent et al.,* 2005; *Thompson et al.,* 2006]. These areas have a lower abundance of rocks than the background mare or highland regolith, suggesting a greater degree of ejecta fragmentation than might be expected. Over time, smaller impacts excavate more blocks from the underlying material, and the radar-dark haloes disappear. This offers potential new information on relative crater ages, independent of surface optical properties that can vary with target composition and regolith maturity [e.g., *Hawke et al.,* 2004].

At the basin scale, the radar echoes show that melt-rich ejecta from Orientale (likely the last large basin to form) fills local lows and crater floors across much of the Moon's south polar area [*Campbell and Campbell,* 2006]. This ponded material provides a fresh source of fragmental debris for small craters, with the result that apparently old, large crater floors have abundant superposed small craters with rugged ejecta. The radar data provide a view of the subsurface physical properties of the regolith and delineate the melt-rich materials as a time-stratigraphic unit without reference to crater counts complicated by the lack of clear distinction between small primary and secondary craters.

Finally, the 70-centimeter images reveal new details of glass-rich pyroclastic deposits, which may contain resource-level concentrations of volatiles. The Aristarchus Plateau is the largest of these features (Figure 3), but there are other significant occurrences, such as those along the rim of Mare Serenitatis. Variations in echo properties across pyroclastic deposits are due to some combination of changes in mantling layer thickness, the roughness of the underlying terrain, and the presence of blocky ejecta from nearby craters. Further work will constrain these factors and yield estimates of the pyroclastic thickness and accessibility (lack of numerous included rocks) for resource exploitation.

Onward to Mars

The new lunar maps show the complementary nature of long-wavelength radar observations and other remote sensing measurements. For the Moon, the thickness of the impact-gardened layer means that most applications focus on the properties of the mixed rock and dust. On Mars, however, there are many areas where important geologic features are obscured by centimeters to meters of fine sediment. A long-wavelength orbital radar sensor could look beneath these mantling materials to reveal ancient terrain sculpted by impacts, volcanism, wind, water, and ice.

Acknowledgments

The authors thank the staff of Arecibo and the GBT, especially A. Hine and F. Ghigo, for invaluable assistance. Arecibo Observatory is part of the National Astronomy and Ionosphere Center, operated by Cornell University under a cooperative agreement with the NSF. The GBT is part of the National Radio Astronomy Observatory, an NSF facility operated by Associated Universities, Inc. J. Chandler (Smithsonian Astrophysical Observatory) provided observing ephemerides. This work was supported in part by grants from NASA's Planetary Astronomy and Planetary Geology and Geophysics programs.

References

Campbell, B. A., and D. B. Campbell (2006), Surface properties in the south polar region of the Moon from 70-cm radar polarimetry, *Icarus, 180,* 1–7.

Campbell, B. A., and B. R. Hawke (2005), Radar mapping of lunar cryptomaria east of Orientale basin, *J. Geophys. Res., 110,* E09002, doi:10.1029/2005JE002425.

Carrier, W. D., Olhoeft, G. R. and Mendell, W., Physical properties of the lunar surface. In: Lunar Sourcebook. Cambridge Univ. Press, New York, 1991.

Ghent, R. R., D. W. Leverington, B. A. Campbell, B. R. Hawke, and D. B. Campbell (2005), Earth-based observations of radar-dark crater haloes on the Moon: Implications for regolith properties, *J. Geophys. Res., 110,* E02005, doi:10.1029/2004JE002366.

Hawke, B. R., D. T. Blewett, P. G. Lucey, J. F. Bell, B. A. Campbell, and M. S. Robinson (2004), The origin of lunar crater rays, *Icarus, 170,* 1–16.

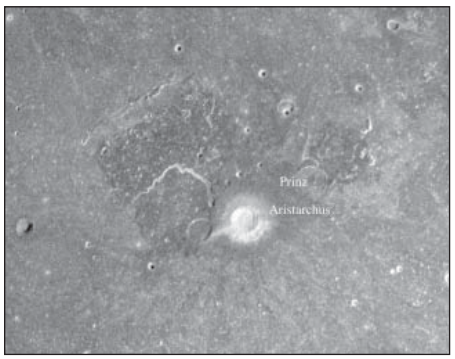

Fig. 3. Seventy-centimeter radar map of the Aristarchus Plateau; opposite-sense circular polarization. Aristarchus crater is 40 kilometers in diameter. Pyroclastic deposits across the Plateau and northeast of crater Prinz are radar-dark, due to a combination of fine-grained material and possible higher electrical losses. Variations in the radar brightness may reflect changes in deposit thickness. Subtle radar-dark 'rays' extend from Aristarchus, complementing the low-return halo seen for this and other large, young lunar craters.

Mustard, J. F., and J. W. Head (1996), Buried stratigraphic relationships along the southwestern shores of Oceanus Procellarum: Implications for early lunar volcanism, *J. Geophys. Res., 101,* 18,913–18,925.
Schaber, G. G., T. W. Thompson, and S. H. Zisk (1975), Lava flows in Mare Imbrium: An evaluation of anomalously low Earth-based radar reflectivity, *Moon, 13,* 395–423.
Thompson, T. W. (1987), High-resolution lunar radar map at 70-cm wavelength, *Earth Moon Planets, 37,* 59–70.
Thompson, T. W., B. A. Campbell, R. R. Ghent, B. R. Hawke, and D. W. Leverington (2006), Radar probing of planetary regoliths: An example from the northern rim of Imbrium Basin, *J. Geophys. Res., 111,* E06S14, doi:10.1029/2005JE002566.

Author Information

Bruce A. Campbell, Center for Earth and Planetary Studies, Smithsonian Institution, Washington, D. C.; E-mail: campbellb@si.edu; Donald B. Campbell and Jean-Luc Margot, Department of Astronomy, Cornell University, Ithaca, N.Y.; Rebecca R. Ghent, Department of Geology, University of Toronto, Ontario, Canada; Michael Nolan, Arecibo Observatory, Arecibo, Puerto Rico; Lynn M. Carter, Center for Earth and Planetary Studies, Smithsonian Institution; and Nicholas J. S. Stacy, Defence Science and Technology Organization, Edinburgh, Australia.

Online Analysis Enhances Use of NASA Earth Science Data

PAGES 14, 17

Giovanni, the Goddard Earth Sciences Data and Information Services Center (GES DISC) Interactive Online Visualization and Analysis Infrastructure, has provided researchers with advanced capabilities to perform data exploration and analysis with observational data from NASA Earth observation satellites. In the past 5–10 years, examining geophysical events and processes with remote-sensing data required a multistep process of data discovery, data acquisition, data management, and ultimately data analysis. Giovanni accelerates this process by enabling basic visualization and analysis directly on the World Wide Web. In the last two years, Giovanni has added new data acquisition functions and expanded analysis options to increase its usefulness to the Earth science research community.

The most commonly used visualizations in Giovanni are area maps, time-series plots, latitude versus time or longitude versus time Hovmöller plots, and vertical profiles for some atmospheric data products. The primary data consist of global gridded data sets with reduced spatial resolution. Basic analytical functions performed by Giovanni currently are carried out by the Grid Analysis and Display System (GrADS). Numeric data output from each visualization or statistical plot can be obtained in a single step and utilized in other analytical software packages.

Giovanni allows researchers the ability to rapidly explore data, so that spatial-temporal variability, anomalous conditions, and patterns of interest can be directly analyzed online before optional downloading of higher resolution data.

Case Study: Analyzing a Saharan Dust Storm

Figure 1 shows an example of Giovanni visualizations, a Saharan dust storm that occurred on 30 April 2003. The Moderate Resolution Imaging Spectroradiometer (MODIS) on the Aqua satellite observed this storm, when a powerful dust-laden surge of superheated, desiccative air from Mauritania surged over the coast of Senegal and the Atlantic Ocean.

Such dust storms are known to influence biogeochemical and meteorological processes. Iron in the mineral aerosols may initiate or augment phytoplankton blooms, or provide micronutrients to the South and Central American rain forest canopy. Dust-borne bacteria may induce coral diseases in Caribbean reefs, and dust aerosols may affect hurricane formation. Therefore, scientists examining the striking image of the storm (Figure 1a) might immediately want to characterize it, asking questions such as: How thick was the dust in this outbreak? How often did Saharan dust storms in early 2003 carry dust over the Atlantic Ocean, and how far? How dry was the air carrying the dust, and what altitude did this dry mass of air reach?

To investigate this Saharan dust plume, atmospheric scientists can use Giovanni on MODIS data to generate an aerosol optical depth (AOD) map of the dust plume (Figure 1b); a Hovmöller latitude versus time plot of AOD from late April to early May 2003 (Figure 1c); and a time series of dust outbreaks from February to May 2003 (Figure 1d).

Giovanni provides access to data from other sensors, including the Atmospheric Infrared Sounder (AIRS) on the Aqua satellite. AIRS provides a relative humidity profile plotted against latitude (Figure 1e). The map and time series of AOD, combined with the humidity profile, provide a four-dimensional depiction of Saharan dust outbreaks in early 2003, accomplished in minutes on the Web, without the need to order, transfer, or extract a single data file.

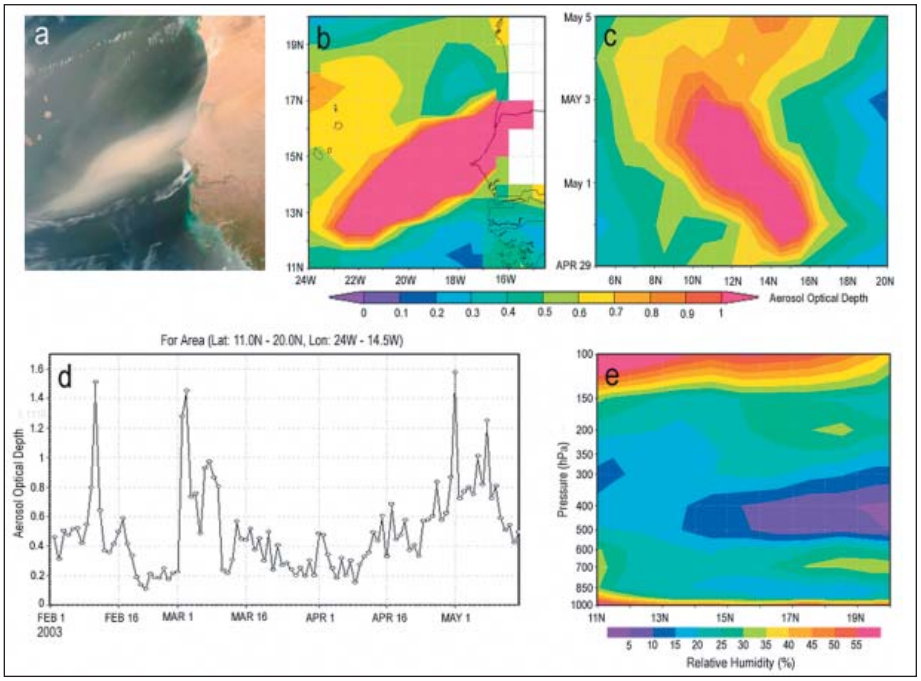

Fig. 1. (a) MODIS-Aqua image of Saharan dust storm, 30 April 2003. The Cape Verde islands are at left. Dakar, Senegal, is the hook-shaped peninsula under the dust cloud on the coast, and coastal wetlands of Gambia and Guinea-Bissau are at the bottom. (b) Aerosol optical depth (AOD) map of this event from MODIS-Terra data. (c) Hovmöller latitude versus time plot of MODIS-Terra AOD for late April and early May 2003, showing the initial southern direction of dust movement. (d) MODIS-Terra AOD time series for February to mid-May 2003, showing that another large dust storm occurred in February. (e) Atmospheric Infrared Sounder (AIRS) relative humidity atmospheric profile plotted against latitude, showing the penetration of dry Saharan air with the dust storm over the Atlantic Ocean. The data plots are original Giovanni output; axis and color bar labels have been modified for legibility.

By J. G. Acker and G. Leptoukh